A Comparative Study of Three Fault Diagnosis Schemes for Wind Turbines

Satadru Dey, *Student Member, IEEE*, Pierluigi Pisu, *Member, IEEE*, and Beshah Ayalew

***Abstract*— In wind turbine systems, early diagnosis and accommodation of faults are crucial for the reliable and cost effective operation of wind turbines and their success as viable renewable energy conversion solutions. This paper proposes and compares three different diagnostic schemes that address the issue of fault detection and isolation for the drivetrain and generator–converter subsystems of a wind turbine. The first diagnostic scheme is based on a cascade of two Kalman filters intended to alleviate the effect of the nonlinear aerodynamic torque generation in the drivetrain dynamics. The second scheme uses a bank of dedicated observers, each of which exploits Thau's argument for systems featuring nonlinear static feedback. The third scheme is a secondary H_∞ filtering mechanism constructed from parity equations by treating the nonlinearity as bounded uncertainty. The performance of each scheme is demonstrated using simulations of the wind turbine system. Robustness of the schemes has been analyzed in terms of parametric uncertainties and different operating conditions. A detailed comparison is also presented pointing to the positive and negative aspects of each scheme.**

***Index Terms*— Cascaded observers, dedicated observers, fault detection and isolation, H-infinity diagnostic filter, Kalman filter, wind turbines.**

NOMENCLATURE

A	System matrix.
B	Input matrix.
B_{dt}	Torsion damping coefficient of the drive train.
B_r	Viscous friction of the rotor shaft.
B_g	Viscous friction of the generator shaft.
C_q	Torque coefficient table.
F	Filter transfer function.
G	Process noise matrix for state equation.
H	Process noise matrix for output equation.
J_g	Moment of inertia of generator shaft.
J_r	Moment of inertia of rotor shaft.
K	Uncertain gain.
K_{dt}	Torsion stiffness of the drivetrain.
L	Observer gain.
N	Coupled noise covariance matrix.
N_g	Gear ratio.
P_g	Generator power.
$P_{g,m}$	Generator power measurement.
Q	Process noise covariance matrix.
$\hat{R}$	Measurement noise covariance matrix.
$\bar{R}$	Rotor radius.
R	Residual.
$r_{\omega g P}$	Residual from power sensor.
$r_{\omega r 1}$	Residual for rotor speed sensor.
$r_{\omega g 1}$	Residual for generator speed sensor.
r_{τ_g}	Residual for actuator in generator–converter.
$r_{\omega r 1 f}$	Filtered residual 1.
$r_{\omega r 2 f}$	Filtered residual 2.
T_{rg}	Transfer matrix for the drivetrain system.
$T_{\omega_r \tau_r}$	Transfer matrix from aerodynamic torque to rotor speed.
$T_{\omega_g \tau_r}$	Transfer matrix from generator torque to rotor speed.
T_{zf}	Transfer matrix from fault to final residuals.
T_{yf}	Transfer matrix from fault to primary residuals.
T_{yd}	Transfer matrix from disturbance to final residuals.
u	System input.
v_w	Wind speed.
x_{est}	Estimated states.
y_{est}	Estimated outputs.
τ_r	Aerodynamic torque.
τ_g	Generator torque.
$\tau_{g,m}$	Generator torque measurement.
$\tau_{g,r}$	Aerodynamic torque reference.
$\hat{\tau}_g$	Generator torque estimate.
$\hat{\tau}_r$	Aerodynamic torque estimate.
$\tau_{g,\mathrm{est}}$	Generator torque estimate.
$\tau_{r,\mathrm{est}}$	Aerodynamic torque estimate.
ω_r	Rotor speed.
ω_g	Generator speed.
$\omega_{r,m}$	Rotor speed measurement.
$\omega_{g,m}$	Generator speed measurement.
$\hat{\omega}_g$	Generator speed estimate.
$\hat{\omega}_r$	Rotor speed estimate.
ω_n	System natural frequency.
β	Pitch angle.
ζ	System damping ratio.
ρ	Wind density.
λ	Break frequency.
η	Drivetrain efficiency.
η_g	Generator efficiency.
θ_Δ	Torsion angle.
χ	Torque speed gradient function.
α_{gc}	Parameter of first-order actuator dynamics.
$\alpha_{\omega_{r\eta}}$	Desired filter parameter.

Manuscript received May 28, 2014; revised September 26, 2014; accepted December 31, 2014. Manuscript received in final form January 6, 2015. Recommended by Associate Editor X. Zhang.

S. Dey and P. Pisu are with the Department of Automotive Engineering, Clemson University, Clemson, SC 29634 USA (e-mail: satadrd@clemson.edu; pisup@clemson.edu).

B. Ayalew is with the Clemson University-International Center for Automotive Research, Greenville, SC 29607 USA (e-mail: beshah@clemson.edu).

Color versions of one or more of the figures in this paper are available online at http://ieeexplore.ieee.org.

Digital Object Identifier 10.1109/TCST.2015.2389713

$\alpha_{\omega_{g\eta}}$ Desired filter parameter.
α_{ω_r} Desired filter parameter.
α_1 Weighing factor for residuals.
α_2 Weighing factor for residuals.

I. Introduction

WIND energy remains an important alternative among truly renewable energy resources. However, the nonlinear aerodynamics and the stochastic nature of wind require complex control systems to maximize energy production and ensure reliable operation. Over the past few years, large wind turbines are being built and installed in offshore areas due to land use and noise issues [1]. The maintenance and repair costs are larger in offshore turbines compared with their onshore counterparts. Therefore, for cost effective energy production, it is very important to ensure the availability and reliability of the system by reducing downtime and cost per failure. Herein lies the importance of fault diagnosis and fault-tolerant schemes, where reliability and availability can be enhanced with early detection and reconfiguration of faulty parts and control actions.

Wind turbine is a complex system comprised of different components or parts (e.g., blades, generators, gearbox, rotor, and tower). A volume of literature exists on fault diagnostic schemes designed for specific parts considering the detailed part dynamics. For example, a wavelet transform-based method [2], observer-based scheme [3], [4] for generator faults, and diagnostic schemes [5], [6] for wind turbine gearboxes are presented. Instead of designing diagnostic schemes for individual parts, the diagnostic problem can also be treated at the subsystem level by segregating the overall wind turbine into several subsystems with simplified dynamics (e.g., drivetrain subsystem, blade and pitch subsystem, generator and converter subsystem, and controller subsystem). Such wind turbine models can be found in [7]–[9].

There are some review works on wind turbine diagnostics in the literature. In [10], a brief review of existing diagnosis schemes can be found; however, no qualitative comparison of the schemes has been provided. Pourmohammad and Fekih [11] concentrated only on fault tolerant control and discusses the state of the art and future scope. The existing approaches for wind turbine fault diagnosis can be broadly categorized into two categories: 1) data-driven approach and 2) physical model-based approach. Among the data-driven approaches, a fuzzy system-based method [12], subspace identification method [13], support vector machine-based method [14], and set theoretic approach [15] have been presented. In general, the disadvantage with data-driven schemes lies in the extensive training needed for the classification algorithm and the associated requirement for large amount of data.

As the name indicates, in physical model-based schemes, a system model is used to detect, isolate, and subsequently accommodate the faults. An advantage of most of the model-based schemes is the ability to deal with unforeseen fault scenarios using model predictions without requiring large sets of data. Different model-based diagnostics approaches exist in the current literature. In [16], after generating primary residuals using a model-based approach and physical redundancies, a counter-based thresholding method is used for wind turbine fault diagnosis. In [17], an observer-based fault detection scheme has been presented, where the residual evaluation is done by a generalized likelihood ratio test and a cumulative variance index. An estimation-based approach is given in [18]. Kiasi *et al.* [19] proposed an unscented Kalman filter approach; however, the computational burden could be high for such scheme in real-time implementation. Odgaard and Stoustrup [20], [21] constructed an unknown input observer approach for sensor fault detection and extended this approach for fault-tolerant control. In a previous paper, Pisu and Ayalew [22] designed a secondary robust H_∞ filtering scheme for diagnostics of both the blade pitch and drivetrain systems. In [23], a parameter estimation technique (block least square) is used to estimate the faults. However, this approach could be computationally expensive and could create some issues if the matrix is ill-conditioned. In [8] and [24], an informative and critical comparative study of the existing diagnostic approaches is given. There are some issues listed in the existing model-based approaches, e.g., large number of false alarm for some faults in [18], slow detection time in [17], and requirements of significant time and knowledge in [16]. There are some other schemes, which detect/isolate only actuator faults [13], only sensor faults [14], [15]. In [29], a proportional multiple integral observer is used only for sensor fault detection. However, they did not consider all the components altogether (sensor, actuator, and system parameter). Moreover, most of the approaches did not consider parametric faults of the drivetrain system. Finally, in wind turbine drivetrain, the aerodynamic torque measurement is not available and the dependence of aerodynamic torque on rotor speed creates a coupling in the dynamics. Most of the existing approaches do not take this coupling into consideration, while designing the diagnostic scheme. Moreover, there is a nonlinear dependency of the aerodynamic torque on the wind speed.

The main contributions of this paper are discussions of two new proposed schemes along with a third scheme which was proposed in [22] and exploration of their potential to address the issues discussed in the previous paragraph. A comparative study is provided between these three schemes in terms of different aspects of detectability, computation burden, and design complexity. This comparative study is different from the one given in [24], where a comparison of already existing schemes [14], [16]–[18] is given.

In this paper, we focus on the fault diagnosis of the drivetrain and generator–converter subsystems of the wind turbine. The main challenges in designing a diagnostic scheme for these subsystems are: 1) the aerodynamic torque measurement is not available and the dependence of aerodynamic torque on rotor speed creates a coupling and 2) the aerodynamic torque also nonlinearly depends on wind speed and wind speed measurements are subject to significant noise. Here, we assume that the wind speed is known via measurement or some estimation technique [29] and focus on the first challenge. In addition to these issues, if there is a fault-tolerant scheme in

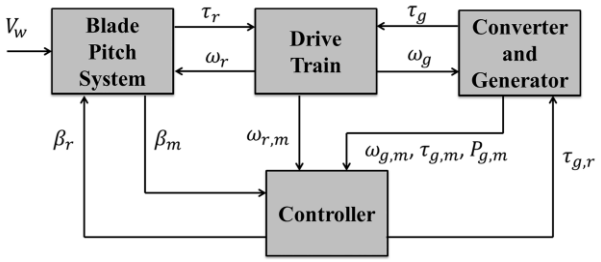

Fig. 1. Wind turbine system diagram.

the control system, the detection of faults will be influenced by the coupling between the wind turbine and fault-tolerant controller. However, in this paper, we assume that there is no fault-tolerant scheme in the control system and we focus only on the fault detection and isolation problem.

As discussed earlier, each of the three schemes considers the mentioned coupling and tries to address it. The first approach uses a cascade of two Kalman filters to detect and isolate several faults. In this case, an aerodynamic torque estimator (consisting of an algebraic map and a Kalman filter that treats the aerodynamic torque as unknown disturbance) is used, which subsequently provides the aerodynamic torque estimate as a known input to the second Kalman filter of the cascade. In the second approach, a dedicated observer-based scheme is used, where a bank of observers are applied each using a different sensor measurement. Then, by comparing the estimates from different observers, the diagnostic problem is solved. The design of the dedicated observer is based only on the linear dynamics of the system (ignoring the nonlinearity as unknown disturbance) and the convergence of the estimation error dynamics is verified for the overall nonlinear system using Thau's argument [30]. The third approach treats the nonlinearity as an uncertainty by constructing a secondary robust H_∞ filtering scheme acting on primary residual signals generated via parity equations. The three schemes are compared for their positive and negative aspects, considering particular diagnostic problems in the wind turbine drivetrain and converter–generator subsystems.

The paper is organized as follows. Section II gives a brief description of the wind turbine system and its model. Section III outlines the diagnostic problem considered in this paper with specific types of faults in sensors, actuators, and parameters for the wind turbine system. Section IV presents the details of the three diagnosis schemes briefly described above. In Section V, robustness of the schemes has been analyzed in terms of parametric uncertainties and different operating conditions. Moreover, a comparative discussion of the three schemes has been presented. Finally, Section VI provides the conclusion of this paper along with open problems and future work.

II. Wind Turbine Model

A system diagram of the three-blade horizontal axis wind turbine is shown in Fig. 1. It consists of four main subsystems: 1) the blade pitch subsystem; 2) generator and converter subsystem; 3) drivetrain subsystem; and 4) the controller. The controller receives the sensor measurements and computes the reference pitch angles and the reference generator torque. The controller works in four different modes based on operating condition of the wind turbine, which are startup, power optimization, constant power, and high wind speed zones. The available sensor measurements are: two pitch sensors for each blade of the turbine, two speed sensors for rotor speed, two speed sensors for generator speed, one generator power sensor, one generator torque sensor, and one wind speed sensor.

For detail descriptions of the working principle of the whole wind turbine system one may consult [31]. For this paper, the following model layout is directly adopted from [7], which defined benchmark problems for wind turbine fault detection and isolation.

A. Blade Pitch Subsystem

The blade subsystem is acted upon by the wind and produces the aerodynamic torque. We assume the blade pitch angles are available via fault-free sensor measurements. The aerodynamic torque produced by the wind turbine blades are given as

$$\tau_r(t) = \sum_{i=1}^{3} \frac{\rho \pi \bar{R}^3 C_q(\lambda(t), \beta_i(t)) v_w^2(t)}{2} \tag{1}$$

where $\lambda = \omega_r \bar{R}/v_w$ is the tip speed ratio and C_q is the torque coefficient, which is a (assumed) known, nonlinear function (map) of tip speed ratio and pitch angles. This dependence of the aerodynamic torque on rotor speed gives rise to an inherent algebraic (static) feedback into the drivetrain model.

Note: The mapping (1) uses torque coefficient C_q which is uncertain. However, two of the proposed schemes (the cascaded Kalman filter-based scheme and especially the robust H_∞ scheme) have the inherent capability of handling some bounded uncertainty, whereas the dedicated observer-based scheme is not effective when the uncertainty is high.

B. Drivetrain Subsystem

The drivetrain is modeled as a coupled two-mass system (rotor blades on one side and generator on another, connected by a flexible shaft). The model is given in the state-space form as

$$\begin{bmatrix} \dot{\omega}_r \\ \dot{\omega}_g \\ \dot{\theta}_\Delta \end{bmatrix} = \begin{bmatrix} -\dfrac{B_{\mathrm{dt}} - B_r}{J_r} & -\dfrac{B_{\mathrm{dt}}}{N_g J_r} & -\dfrac{K_{\mathrm{dt}}}{J_r} \\ \dfrac{\eta B_{\mathrm{dt}}}{N_g J_g} & -\dfrac{\eta B_{\mathrm{dt}}}{N_g^2 J_g} - \dfrac{\eta K_{\mathrm{dt}}}{J_g} & \dfrac{\eta K_{\mathrm{dt}}}{N_g J_g} \\ 1 & -\dfrac{1}{N_g} & 0 \end{bmatrix} \begin{bmatrix} \omega_r \\ \omega_g \\ \theta_\Delta \end{bmatrix} + \begin{bmatrix} \dfrac{1}{J_r} & 0 \\ 0 & -\dfrac{1}{J_g} \\ 0 & 0 \end{bmatrix} \begin{bmatrix} \tau_r \\ \tau_g \end{bmatrix}. \tag{2}$$

TABLE I
FAULT INJECTION SCENARIO FOR DIAGNOSTIC SCHEME TESTING

Fault Injection Time (s)	Fault Scenario
1000-1100	Simultaneous scaling error sensor faults of rotor speed sensor 2 and generator speed sensor 2
1500-1600	Single sensor stuck fault of rotor speed sensor 1
3800-3900	Bias fault in converter actuator
4000-4200	Drivetrain efficiency change

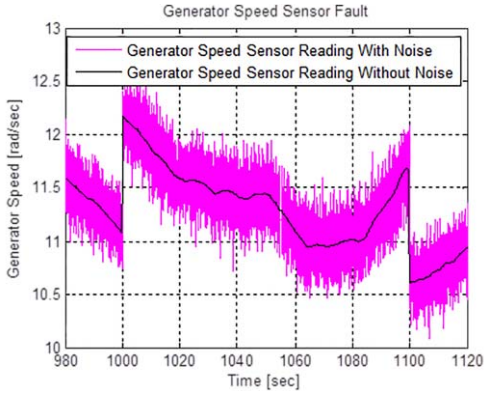

Fig. 2. Generator speed sensor 2 scaling error fault with noise.

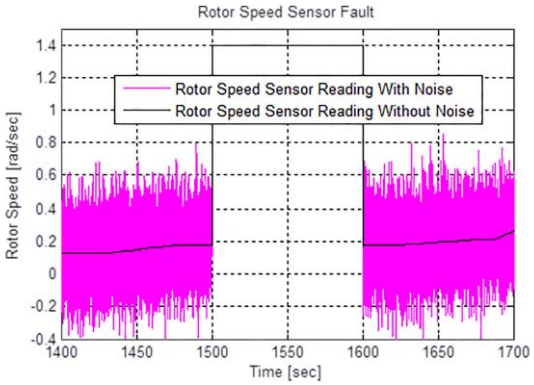

Fig. 3. Rotor speed sensor 1 stuck fault with noise.

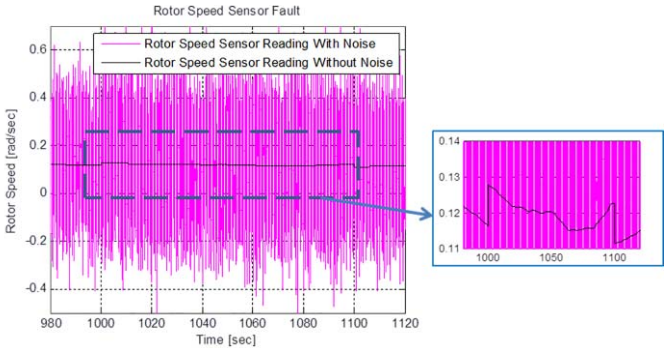

Fig. 4. Rotor speed sensor 2 scaling error fault with noise.

C. Generator and Converter Subsystem

The generator is provided with a reference torque input by the controller. The generator and converter system is modeled as a first-order dynamics given by

$$\frac{\tau_g(s)}{\tau_{g,r}(s)} = \frac{\alpha_{gc}}{s+\alpha_{gc}}. \tag{3}$$

The generator power is given by

$$P_g(t) = \eta_g \omega_g(t) \tau_g(t). \tag{4}$$

III. DIAGNOSTIC PROBLEMS

In the given wind turbine, many possible faults can occur in each of the subsystems. For the purposes of this paper, we focus on the faults in the drivetrain and generator–converter subsystems. Possible faults considered in this paper are described in the following. Two types of faults are considered for rotor and generator speed sensors. The first fault is the sensor stuck fault and the second fault is a scaling error fault in the sensor reading. In addition, one case of simultaneous faults, in rotor speed and generator speed sensors is considered. The actuator fault (bias type fault) considered here is the case where the output generator torque does not follow the commanded generator torque. A parametric fault is considered as drivetrain efficiency fault that changes in drivetrain dynamics, possibly due to wear and tear. Table I summarizes the fault scenarios to be considered. Some of the fault simulations are shown in Fig. 2 (a scaling fault in generator speed sensor 2), Fig. 3 (a stuck-type fault is shown in rotor speed sensor 1), and Fig. 4 (scaling fault in rotor speed sensor 2).

There are some typical concerns in wind turbine system diagnostics. One of the major problems is that measurements are often associated with a high noise level. Sometimes the faults may be embedded inside the noise resulting in low fault-to-noise signal ratio, which makes the detection difficult (refer to the fault considered in Fig. 4). Furthermore, a major source of nonlinearity comes from the dependence of the aerodynamic torque on rotor speed via the torque coefficient (a nonlinear map). This represents an inherent nonlinear algebraic feedback in the wind turbine drivetrain subsystem.

IV. DIAGNOSTIC SCHEMES

A. Diagnostic Scheme 1: Cascaded Kalman Filter-Based Approach

First, let's recall the basic idea of using Kalman filters for fault detection. We estimate system states using modeled information via a Kalman filter and compare them with sensor measurements. In discrete time, this essentially involves monitoring the properties of the innovation sequence of the filter [32]. In normal operating conditions, the innovation sequence, which is the difference between sensor measurements and filter estimates, is used as residual. The residual has zero mean property under nonfaulty condition whereas sensor faults affect the residual (innovation sequence) by changing it from its zero mean nature. The Kalman filter is tuned in such a way that the sensor faults are treated

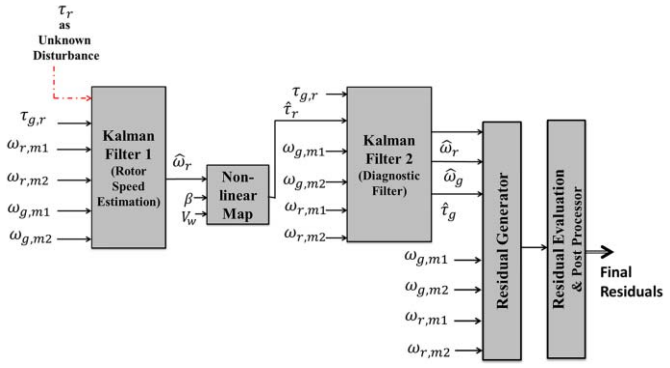

Fig. 5. Diagnostic filter scheme based on Kalman filters.

as output disturbances and the filter rejects the disturbances providing an accurate/nonfaulty state estimate, provided that the nature of the faults are within the bound of noise properties defined with noise covariance matrices for the Kalman filter design.

As discussed earlier, the aerodynamic torque is a nonlinear function of rotor speed and other variables

$$\tau_r(t) = \sum_{i=1}^{3} \frac{\rho \pi \bar{R}^3 C_q(\lambda(t), \beta_i(t)) v_w^2(t)}{2}$$
$$\Rightarrow \tau_r(t) = f(t, \omega_r, v_w)$$

where $f(.)$ is a nonlinear map, which is assumed known for the wind turbine under consideration. To deal with this nonlinearity, others have proposed schemes using unscented Kalman filter [19], unknown input observer [20]. These approaches resort to intensive design of the observer gains, which is avoided in this paper by formulating the system in a different way. Here, we implement the cascade structure in Fig. 5, using a sequence of two standard linear Kalman filters. The nonlinearity of the system is accommodated using an aerodynamic torque estimator, which consists of a Kalman filter (Kalman filter 1 in Fig. 5) and a nonlinear algebraic map in cascade. Kalman filter 1 estimates the rotor speed and then the algebraic map calculates the aerodynamic torque based on the estimated rotor speed. This estimated aerodynamic torque is fed to the diagnostic filter (Kalman filter 2 in Fig. 5) as a known input and then the state estimates from the diagnostic filter (Kalman filter 2) are compared with the sensor information to generate residuals.

While designing Kalman filter 1, the aerodynamic torque, which is an input to the system, was treated as an unknown disturbance by breaking the inherent algebraic loop between rotor speed and aerodynamic torque. The resulting system dynamics is linear and the Kalman gains can be designed based on this linear system, with aerodynamic torque as an unknown disturbance. While implementing the filter, the aerodynamic torque coming out of the nonlinear map is fed back as the disturbance term discussed above. This configuration makes the implementation (not the design) nonlinear and convergence can be verified by the conditions given in [33], which involve bounds in initial estimation error, smoothness of the nonlinear term, and invertibility of process noise matrix.

One may wonder whether Kalman filter 1 could not be sufficient for use as a diagnostic filter by estimating all states in one step. However, it was observed in simulations that, with the aerodynamic torque treated as an unknown disturbance, the designed filter does a poor job of estimating system states other than the rotor speed. Through the use of the second Kalman filter, which treats the aerodynamic torque as a known input, the estimation accuracy of all states was greatly improved.

To complete the design of the Kalman filters, the state-space model of the drivetrain is modified by augmenting another state corresponding to the generator actuator's first-order dynamics. The augmented generator actuator state will be used later to detect actuator faults. The modified state-space model is given as

$$\begin{bmatrix} \dot{\omega}_r \\ \dot{\omega}_g \\ \dot{\theta}_\Delta \\ \dot{\tau}_g \end{bmatrix} = A \begin{bmatrix} \omega_r \\ \omega_g \\ \theta_\Delta \\ \tau_g \end{bmatrix} + B \begin{bmatrix} \tau_r \\ \tau_{g,r} \end{bmatrix}, \quad \begin{bmatrix} \omega_{r,m1} \\ \omega_{r,m2} \\ \omega_{g,m1} \\ \omega_{g,m2} \end{bmatrix} = C \begin{bmatrix} \omega_r \\ \omega_g \\ \theta_\Delta \\ \tau_g \end{bmatrix}$$

$$A = \begin{bmatrix} -\frac{B_{\rm dt} - B_r}{J_r} & \frac{B_{\rm dt}}{N_g J_r} & -\frac{K_{\rm dt}}{J_r} & 0 \\ \frac{\eta B_{\rm dt}}{N_g J_g} & -\frac{\eta B_{\rm dt}}{N_g^2 J_g} - \frac{B_g}{J_g} & \frac{\eta K_{\rm dt}}{N_g J_g} & -\frac{1}{J_g} \\ 1 & -\frac{1}{N_g} & 0 & 0 \\ 0 & 0 & 0 & -\alpha_{gc} \end{bmatrix}$$

$$B = \begin{bmatrix} \frac{1}{J_r} & 0 \\ 0 & -\frac{1}{J_g} \\ 0 & 0 \\ 0 & \alpha_{gc} \end{bmatrix}, \quad C = \begin{bmatrix} 1 & 0 & 0 & 0 \\ 1 & 0 & 0 & 0 \\ 0 & 1 & 0 & 0 \\ 0 & 1 & 0 & 0 \end{bmatrix}. \tag{5}$$

The general formulation of the discrete time Kalman filter is based on the following process model:

$$x(k+1) = Ax(k) + Bu(k) + Gw(k)$$
$$y(k) = Cx(k) + Du(k) + Hw(k) + v(k) \tag{6}$$

where $x = [\, \omega_r \;\; \omega_g \;\; \theta_\Delta \;\; \tau_g \,]^T$ is the state vector, $u = [\, \tau_r \;\; \tau_{g,r} \,]^T$ is the input vector, $y = [\, \omega_{r,m1} \;\; \omega_{r,m2} \;\; \omega_{g,m1} \;\; \omega_{g,m2} \,]^T$ is the output vector, w is the process noise vector, v is the measurement noise vector; A is the state matrix, B is control input matrix, C is the output matrix, D is the direct transmission matrix, H is the process noise matrix for output, and G is the process noise matrix for state equation. The A, B, C, and D matrices are obtained via Euler discretization of the continuous time state-space model in (5). The GH matrices are determined based on the individual filter's objectives. The noise covariance properties are given as

$$E\{w(k)w(k)^T\} = Q,\ E\{v(k)v(k)^T\} = \hat{R},\ E\{w(k)v(k)^T\} = N.$$

The estimator equation takes the form

$$\hat{x}(k+1/k) = Ax(k/k-1) + Bu(k)$$
$$+ L\{y(k) - C\hat{x}(k/k-1) - Du(k)\} \tag{7}$$

where L is the Kalman gain matrix derived by solving discrete filter algebraic Riccati equation. For Kalman filter 1,

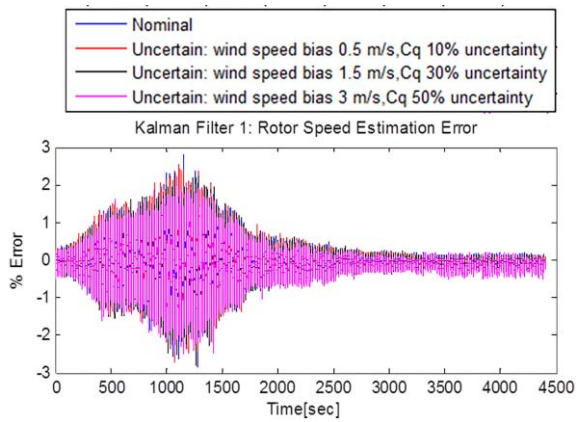

Fig. 6. State estimation error in Kalman filter 1.

the following configuration is chosen:

$$Q = I, \quad \hat{R} = I, \quad N = I, \quad G = \text{diag}[1, \varepsilon, \varepsilon, \varepsilon]$$
$$H = \text{diag}[1, \varepsilon, \varepsilon, \varepsilon]$$

where ε is a small positive number and I is the identity matrix. As discussed earlier, the aerodynamic torque is being treated as an unknown disturbance by choosing the unity term in the (1, 1) element of the process noise matrices.

In case of Kalman filter 2, the aerodynamic torque is assumed to be a known input coming from the aerodynamic torque estimator, which means there is no input disturbance in the system; there are only output disturbances which are basically the sensor faults. The configuration chosen for Kalman filter 2 is

$$Q = I, \quad \hat{R} = I, \quad N = I, \quad G = \text{diag}[\varepsilon, \varepsilon, \varepsilon, \varepsilon]$$
$$H = \text{diag}[\varepsilon, \varepsilon, \varepsilon, \varepsilon].$$

Now, with the stated configuration, the state estimation performance of the two Kalman filters has been analyzed via simulation studies. To evaluate the effectiveness of the Kalman filters, the model has been simulated multiple times along with the filters subjected to a realistic wind sequence given in [7]. In these simulations, along with the nominal condition, model mismatch has also been considered by injecting uncertainties in the most uncertain variables (wind speed measurement and torque coefficient C_q). The estimation errors have been shown in Fig. 6 for Kalman filter 1 and Fig. 7 for Kalman filter 2 under nominal conditions and with various levels of uncertainties. Note that Kalman filter 1 estimate is robust to the considered uncertainties as the estimation error remains within 3% band. This is due to consideration of unknown disturbance in the design. The estimates of Kalman filter 2, especially the rotor and generator speed estimates degrade under uncertainties. This is expected as no input disturbance is considered in the design. However, the estimation errors remain in the band of around 10% most of the time.

The estimation error bounds of the Kalman filters can also be analyzed theoretically under the conditions of satisfying observability rank requirement and sufficiently small initial

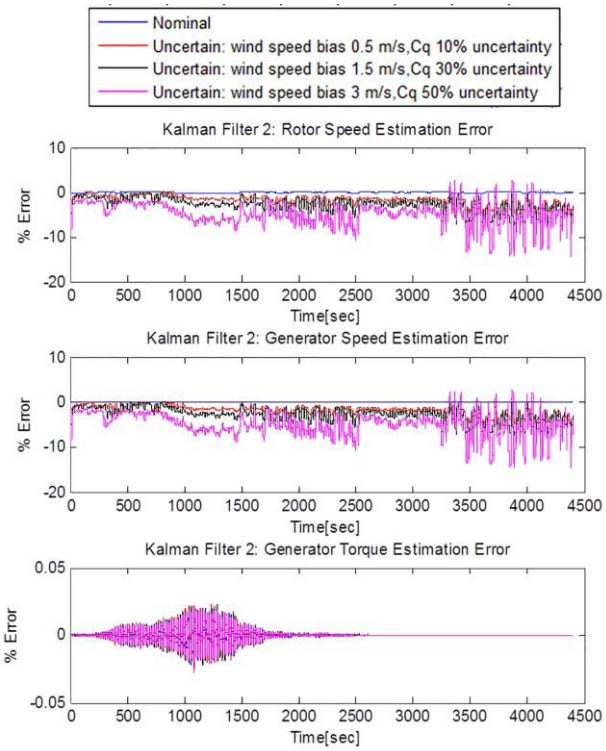

Fig. 7. State estimation error in Kalman filter 2.

TABLE II
RESIDUAL DEFINITIONS IN KALMAN FILTER-BASED DIAGNOSIS SCHEME

Fault	Residual Definition
Rotor speed sensor 1	$R_1 = \widehat{\omega}_r - \omega_{r,m1}$
Rotor speed sensor 2	$R_2 = \widehat{\omega}_r - \omega_{r,m2}$
Generator speed sensor 1	$R_3 = \widehat{\omega}_g - \omega_{g,m1}$
Generator speed sensor 2	$R_4 = \widehat{\omega}_g - \omega_{g,m2}$
Converter actuator	$R_5 = \hat{\tau}_g - \tau_{g,m}$
Drivetrain efficiency	$R_6 = \eta_g \hat{\tau}_g \widehat{\omega}_g - P_{g,m}$
Isolation between generator speed sensors and actuator sensor	$R_7 = \omega_{g,m2} - \omega_{g,m1}$

estimation error and disturbance/noise terms [34]. However, as commented in [34], the estimated error bound is derived based on theoretical sufficient conditions which for the present problem very conservative.

The estimates of rotor speed, generator speed, and generator torque from the diagnostic filter are compared with the sensor measurements to get the residuals for the corresponding sensors. For the drivetrain system parametric (efficiency) fault, generator power sensor is used to generate another residual. This residual is the difference between the estimated power (based on generator torque and speed estimates) and the power sensor measurement. The actuator fault will affect the generator speed, and hence can trigger the residuals for generator speed. To isolate the fault occurrences in generator actuator sensor and speed sensors, an additional residual is used that exploits the difference between the two generator speed sensors. The definitions of the residuals are given in Table II.

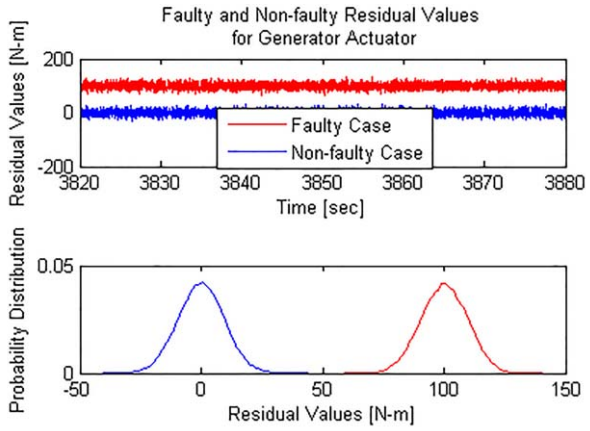

Fig. 8. Generator actuator fault residual samples and probability distribution in faulty and nonfaulty condition.

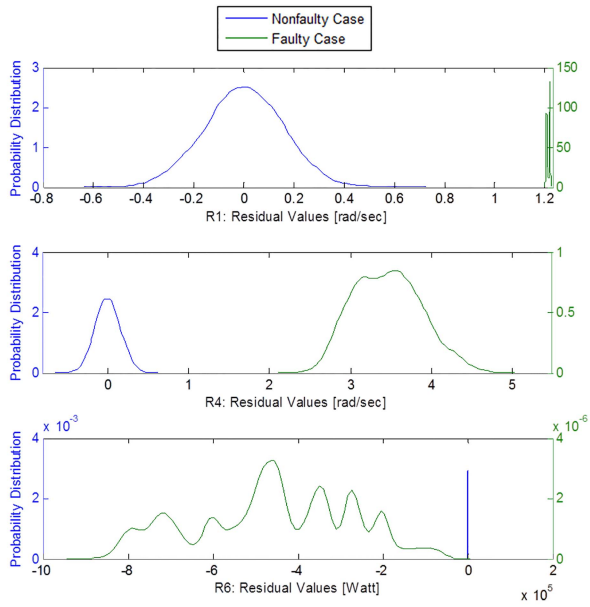

Fig. 9. Residual samples and probability distribution in faulty and nonfaulty condition (R_1, R_4, and R_6).

Due to measurement noise, the residuals do not have the idealized property of being zero even in nonfaulty conditions. Therefore, postprocessing of these residuals is necessary to remove the effect of noise. To select a suitable nonzero threshold, the probability distribution of the residual samples was analyzed under faulty and nonfaulty conditions. The residual value, where the probability distribution curves for two different conditions intersect is selected as the nonzero threshold. The intersection point is chosen to achieve optimality in the sense of equal probability of missed detection and false alarm. The residual samples and their probability distributions for the generator actuator fault residual signal are shown in Fig. 8. In the lower subplot, the probability distributions of the faulty and nonfaulty residuals are shown. The threshold is selected as 50 N · m, which is the intersection point of two distributions.

Similarly, the probability distribution for the residual signals corresponding to rotor speed sensor 1 fault, generator speed sensor 2 fault, and drivetrain efficiency fault are shown in Fig. 9. Note that for all the faults, there is a sufficient

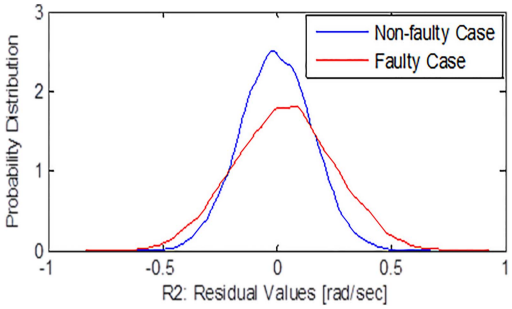

Fig. 10. Rotor speed 2 sensor residual samples and probability distribution in faulty and nonfaulty condition (R_2).

TABLE III
FAULT SIGNATURE TABLE FOR KALMAN FILTER-BASED DIAGNOSIS SCHEME

R_1	R_2	R_3	R_4	R_5	R_6	R_7	Fault Signature
1	0	0	0	0	0	0	$\omega_{r,m1}$
0	1	0	0	0	0	0	$\omega_{r,m2}$
0	0	1	0	0	0	1	$\omega_{g,m1}$
0	0	0	1	0	0	1	$\omega_{g,m2}$
0	0	0	0	1	0	0	$\tau_{g,m}$
×	×	×	×	×	1	×	η

gap between the faulty and nonfaulty probability distribution. However, in case of the rotor speed sensor 2 residual, the faulty and nonfaulty probability distributions are almost inseparable, as shown in Fig. 10. This makes this fault undetectable using this approach. Threshold for all the other residuals have been selected in the intersection of the two probability distributions.

With the information of probability distributions residuals and selection of thresholds, detectability of the considered faults can be analyzed as follows. The residual evaluation logic is given as: residual (r) greater than threshold (th) indicates fault ($f \neq 0$), residual less than or equals to threshold indicates nonfaulty ($f = 0$). Based on this logic, the false alarm rate can be defined as: FAR $= P(r > \text{th}|\ f = 0)$ and the missed detection rate can be defined as: MDR $= P(r < \text{th}|f \neq 0)$. These rates can be computed for each fault from the probability distributions shown in Figs. 8–10. Note that for the rotor speed sensor 1 fault, generator speed sensor 2 fault, generator actuator fault, and drivetrain efficiency fault, there is a significant gap between the faulty and nonfaulty probability distribution. This makes the FAR and MDR almost negligible. In case of rotor speed sensor 2 fault, the FAR and MDR are very high. However, all of these FAR and MDR are valid under the hypothesis that faulty residual probability distributions are the same, as shown in Figs. 8–10. In case of different fault type, size and measurement noise characteristics, these selected thresholds may not be effective if there is significant deviation in the probability distributions. This issue is discussed in detail in Section V.

Finally, a fault signature table, Table III, is generated based on the residual responses to different faults. The residual

TABLE IV
SIMULATION RESULTS FOR KALMAN FILTER-BASED DIAGNOSIS SCHEME

Fault Scenario	Detection/Isolation	Detection Time (s)
Simultaneous scaling error sensor faults of rotor speed sensor 2 and generator speed sensor 2	Only the fault in generator speed sensor 2 is detected. This scheme failed to detect rotor speed sensor 2 fault.	0.1
Single sensor stuck fault of rotor speed sensor 1	Detected and Isolated	0.1
Bias fault in converter actuator	Detected and Isolated	0.1
Drivetrain efficiency change	Detected and Isolated	8.4

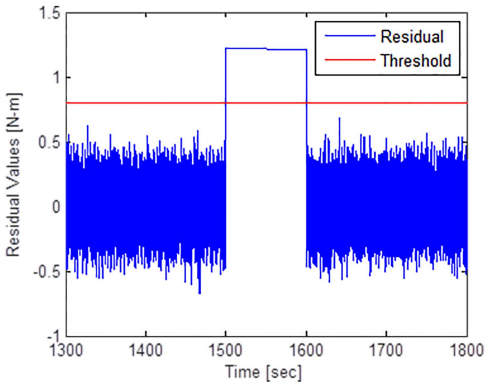

Fig. 11. Residual response (R_1) for rotor speed sensor 1 fault.

values will be below their threshold in the absence of the corresponding fault and cross the threshold in the presence of the fault. In case of drivetrain parameter (efficiency) fault, all the system states will get affected and this will show up in all the measurements. Therefore, this situation might trigger the sensor fault residuals. Because of this reason, there are Xs in other residual signatures when there is a parametric fault. The diagnosis scheme is tested via simulations of a wind turbine model provided in [7] using the fault scenarios described in Section III. The results are listed in Table IV. Simulation sample time is 0.01 s.

One of the residual responses (corresponding to rotor speed sensor 1) is shown in Fig. 11. It is shown that at 1500 s the rotor speed sensor was injected with a stuck-type fault and corresponding residual crossed the threshold after the fault occurrence. It can be observed from Table IV that all the faults are detected and isolated except for the rotor speed sensor 1 fault (for the first fault scenario). This is because this fault is embedded inside the noise signal, i.e., the fault-to-noise signal ratio is very low. As the residuals are defined as the difference between Kalman filter estimates and sensor measurements, the residuals will not be sensitive to faults that are not prominent in the sensor information.

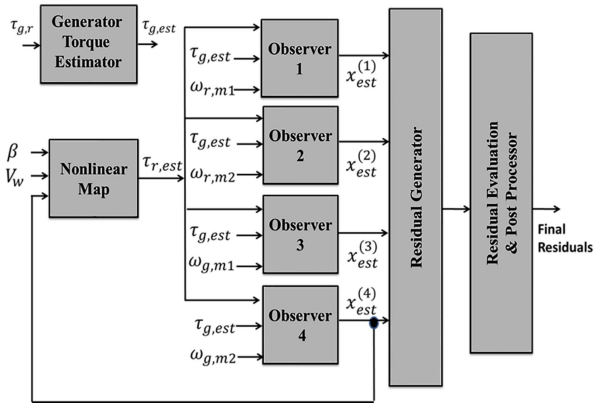

Fig. 12. Diagnostic scheme using dedicated observer setup.

B. Diagnostic Scheme 2: Dedicated Observer-Based Approach

The basic idea of this second scheme is to design a set of observers each of which uses a different sensor measurement to estimate all the states [35]. Then, the differences of the estimated states from different observers are used as primary residuals. If any sensor fault occurs, the corresponding observer, which is using that sensor information to estimate the states will provide faulty estimates thereby producing some nonzero residuals. The overall scheme is shown in Fig. 12. Similar to the Kalman filter-based scheme, a nonlinear algebraic map is used to estimate the aerodynamic torque and that estimate is fed to the dedicated observers. The rotor speed estimate from the observer 4, which is based on generator speed sensor 2, is entered in the algebraic map for the aerodynamic torque.

The state-space model is modified for designing these dedicated observers. As the torsion angle state is not used in our analysis, it is removed to reduce the model order. The modified state-space model is given as

$$\begin{bmatrix} \dot{\omega}_r \\ \dot{\omega}_g \end{bmatrix} = \begin{bmatrix} -\dfrac{B_{\rm dt}-B_r}{J_r} - \dfrac{K_{\rm dt}}{J_r} & \dfrac{B_{\rm dt}}{N_g J_r} + \dfrac{K_{\rm dt}}{N_g J_r} \\ \dfrac{\eta B_{\rm dt}}{N_g J_g} + \dfrac{\eta K_{\rm dt}}{N_g J_g} & -\dfrac{\eta B_{\rm dt}}{N_g^2 J_g} - \dfrac{B_g}{J_g} - \dfrac{\eta K_{\rm dt}}{N_g^2 J_g} \end{bmatrix} \times \begin{bmatrix} \omega_r \\ \omega_g \end{bmatrix} + \begin{bmatrix} \dfrac{1}{J_r} & 0 \\ 0 & -\dfrac{1}{J_g} \end{bmatrix} \begin{bmatrix} \tau_r \\ \tau_{g,est} \end{bmatrix}. \quad (8)$$

For detecting the actuator fault, an estimate of the generator torque is computed using the known first order dynamics of the actuator. The generator torque estimate is given in

$$\tau_{g,\rm est}(s) = \frac{\alpha_{gc}}{s+\alpha_{gc}} \tau_{g,r}(s). \quad (9)$$

The difference between the estimate and the generator torque sensor is defined as the primary residual for the actuator. The estimate that is assumed to produce nonfaulty information all the time is fed to the set of dedicated observers, as shown in (9). This ensures that the dedicated observers are sensitive only to the sensor or parametric faults, not to the actuator fault.

TABLE V
RESIDUAL DEFINITIONS IN DEDICATED OBSERVER-BASED DIAGNOSIS SCHEME

Residual	Residual Definition
Residual 1	$R_1 = x^1_{est} - x^2_{est}$
Residual 2	$R_2 = x^2_{est} - x^3_{est}$
Residual 3	$R_3 = x^3_{est} - x^4_{est}$
Residual 4	$R_4 = x^4_{est} - x^1_{est}$
Residual 5	$R_5 = x^2_{est} - x^4_{est}$
Residual 6	$R_6 = x^1_{est} - x^3_{est}$
Residual 7	$R_7 = P_{g,m} - \eta_g \tau_{g,est} \omega_{g,m1}$
Residual 8	$R_8 = P_{g,m} - \eta_g \tau_{g,est} \omega_{g,m2}$
Actuator Fault Residual	$R = \tau_{g,est} - \tau_{g,m}$

As already discussed earlier, the nonlinear dependence of the aerodynamic torque on rotor speed makes the system dynamics nonlinear. The system state-space model takes the form

$$\dot{x} = Ax + f(x) + Bu \quad y = Cx. \tag{10}$$

In this section, we use the arguments given by Thau's approach [19], where we effectively drop the nonlinear term in (10) and design the observer gains based on the linear dynamics. Given the verifiable observability of the linear part of the system from each sensor measurement considered, and assuming Lipschitz bounds for the nonlinear part, Thau's approach analyzes whether an arbitrary observer gain [which is designed based on only the linear part of (10)] can produce asymptotically stable estimator error dynamics. Thau's argument assumes the observer structure in Luenberger form

$$\dot{\hat{x}} = A\hat{x} + f(\hat{x}) + Bu + L(y - \hat{y}) \quad \hat{y} = C\hat{x}. \tag{11}$$

Following [19], the conditions on the observer gains that asymptotically stabilize the estimation error dynamics can be readily established and verified with the design.

The different observer dynamics are given as follows. Observers 1 and 2 (dedicated to rotor speed sensors 1 and 2)

$$\begin{aligned} \dot{x}^{(j)}_{\text{est}} &= Ax^{(j)}_{\text{est}} + f(\omega_{r,\text{est}}) + B\tau_{g,\text{est}} + L_j\left(\omega^{(i)}_{r,\text{est}} - \omega_{r,mi}\right) \\ y^{(j)}_{\text{est}} &= \omega^{(i)}_{r,\text{est}} \end{aligned} \tag{12}$$

where $i = 1, 2;\ j = 1, 2$. Observers 3 and 4 (dedicated to generator speed sensors 1 and 2)

$$\begin{aligned} \dot{x}^{(j)}_{\text{est}} &= Ax^{(j)}_{\text{est}} + f(\omega_{r,\text{est}}) + B\tau_{g,\text{est}} + L_j\left(\omega^{(i)}_{g,\text{est}} - \omega_{g,mi}\right) \\ y^{(j)}_{\text{est}} &= \omega^{(i)}_{g,\text{est}} \end{aligned} \tag{13}$$

where $i = 1, 2;\ j = 3, 4$.

The definitions of the residuals for the dedicated observer scheme are given in Table V. Residuals R_1–R_6 are used to indicate the rotor and generator speed sensor faults. The details of the residual combinations, which are used to separate different sensor faults, are given in the fault signature tables. The last residual is used for actuator fault detection. Residuals R_7 and R_8, which use the generator power sensor information facilitate isolation in case of multiple sensor faults. In this scheme, we can also detect the generator power sensor fault using either residual R_7 or R_8. This is because we assumed that there cannot be simultaneous faults in both generator speed sensors.

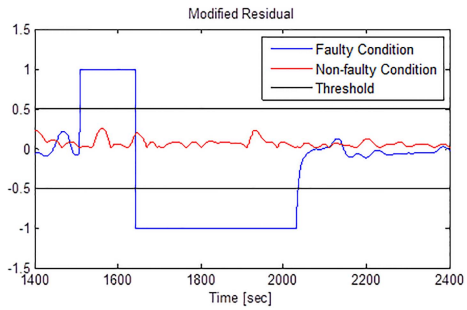

Fig. 13. Faulty and nonfaulty modified residuals.

When observer poles are chosen in such a way as to have a fast estimation, the noise embedded in the sensor information could not be filtered out by the observer. Therefore, the primary residuals coming out of the observer outputs need to be postprocessed to minimize the effect of noise. The postprocessing has been done in two stages. In the first stage, a low-pass filter was used to remove the noise effects. This improved the noise scenario but still was not sufficient. Then, in the second stage, a modified form of residual based on following formula is used to differentiate the faulty and nonfaulty conditions:

$$\bar{R}_1 = \frac{\left(N[R_1(k)]^2 - \sum_{i=k-(N-1)}^{k}[R_1(i)]^2\right)}{N}$$

where N is the width of computation window, k is the current time instant, R_1 is the primary residual, and $\bar{R}_1$ is the modified residual. In the absence of faults, this formula is used to compute the nonfaulty residual. Then, the threshold is selected as 150% of the maximum value of the modified residual computed. It is assumed that the healthy modified residual values under any operating conditions will be below this selected threshold. For a particular residual, the modified residual history for both faulty and nonfaulty cases has been shown in Fig. 13. It can be seen that the nonfaulty modified residual stays below a certain limit, whereas the faulty modified residual shoots up at the occurrence of fault at 1500 s.

Each of the residuals has two components in it since the system model has two states. These two states are combined to make a weighted residual. For example

$$R_{1-\text{weighted}} = \alpha_1 \bar{R}_1(1) + \alpha_2 \bar{R}_1(2). \tag{14}$$

Using this weighing structure, all the residuals have been reduced to have a single component. The fault signatures are given in Table VI.

The results of the dedicated observer-based diagnosis scheme for the fault scenario discussed in Section III are listed in Table VII. Simulation sample time is 0.01 s. Primary residual response (corresponding to rotor speed sensor 1) is shown in Fig. 14. The residual evaluation based on previously discussed modified residual formula is shown in Fig. 15. From the simulation results, it can be seen that all

TABLE VI
FAULT SIGNATURE TABLE FOR DEDICATED OBSERVER-BASED DIAGNOSIS SCHEME

R_1	R_2	R_3	R_4	R_5	R_6	R_7	R_8	R	Fault Signature
1	0	0	1	0	1	0	0	0	$\omega_{r,m1}$
1	1	0	0	1	0	0	0	0	$\omega_{r,m2}$
0	1	1	0	0	1	1	0	0	$\omega_{g,m1}$
0	0	1	1	1	0	0	1	0	$\omega_{g,m2}$
0	0	0	0	0	0	0	0	1	$\tau_{g,m}$
0	1	0	1	1	1	×	×	0	η
0	0	0	0	0	0	1	1	0	$P_{g,m}$

TABLE VII
SIMULATION RESULTS FOR DEDICATED OBSERVER-BASED DIAGNOSIS SCHEME

Fault Scenario	Detection/Isolation	Detection Time (s)
Simultaneous scaling error sensor faults of rotor speed sensor 2 and generator speed sensor 2	Detected, Isolated	80
Single sensor stuck fault of rotor speed sensor 1	Detected, Isolated	7
Bias fault in converter	Detected, Isolated	0.01
Drivetrain efficiency change	Detected, Isolated	22

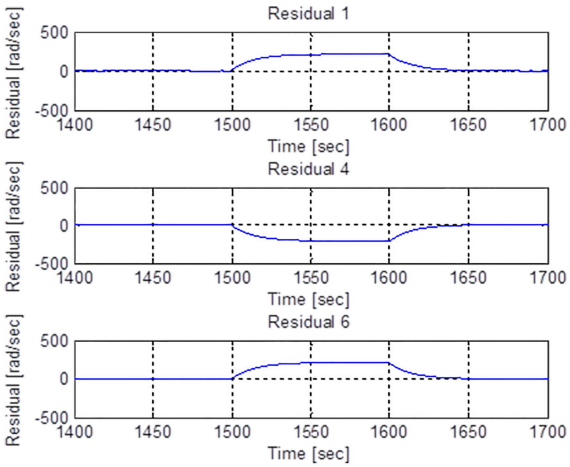

Fig. 14. Primary residual response for rotor speed sensor 1 fault.

the faults are detected using this scheme. The low-pass filtering included to remove noise in the first stage of postprocessing made the proposed scheme slower compared with the Kalman filter-based scheme. The residuals take long time to come back below threshold after the fault is gone. In this time period, when the fault is gone but the residual is still high, we cannot detect another fault.

C. Diagnostic Scheme 3: H_∞ Approach

In this scheme, the parity equation method [36] is used to generate primary residuals, which are then passed through a robust H_∞ filtering scheme to remove the noise effects

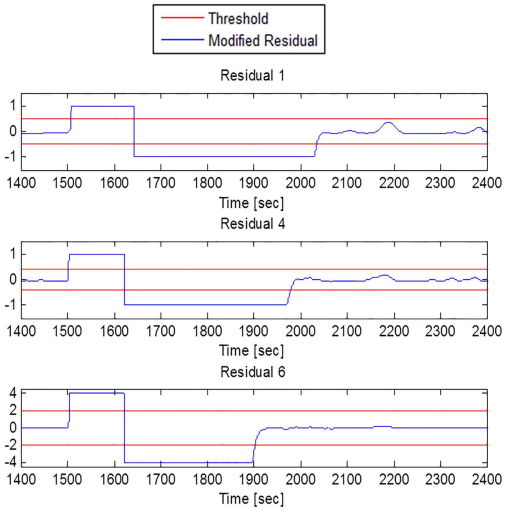

Fig. 15. Modified residual response for rotor speed sensor 1 fault.

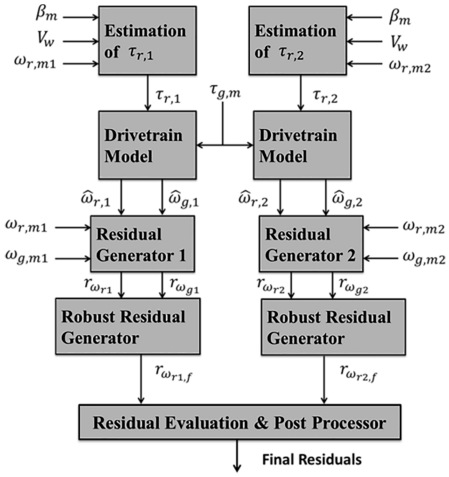

Fig. 16. Diagnostic scheme using parity equation/H_∞ approach.

and undesirable cross coupling between fault-residual pairs. This robust filtering scheme also addresses the issues of aerodynamic nonlinearity and modeling uncertainties.

The overall scheme is shown in Fig. 16. The aerodynamic torque estimate is generated using rotor speed sensor information. Including the possible faults, the overall system equation can be written as

$$\begin{bmatrix} \omega_{r,i}(s) \\ \omega_{g,i}(s) \end{bmatrix} = T_{rg}(s) \begin{bmatrix} \tau_r(s) \\ \tau_g(s) \end{bmatrix} + \Delta T_{rg}(s, \Delta\eta) \begin{bmatrix} \tau_r(s) \\ \tau_g(s) \end{bmatrix} + T_{rg}(s) \begin{bmatrix} 0 \\ \Delta\tau_g(s) \end{bmatrix} + \begin{bmatrix} \Delta\omega_{r,i}(s) \\ \Delta\omega_{g,i}(s) \end{bmatrix}, \quad i = 1, 2. \tag{15}$$

The rotor and generator speed estimates can be written as

$$\begin{bmatrix} \hat{\omega}_{r,i}(s) \\ \hat{\omega}_{g,i}(s) \end{bmatrix} = T_{rg}(s) \begin{bmatrix} \hat{\tau}_{r,i}(s) \\ \tau_g(s) \end{bmatrix} + T_{rg}(s) \begin{bmatrix} 0 \\ \Delta\tau_g(s) \end{bmatrix}, \quad i = 1, 2 \tag{16}$$

where the aerodynamic torque estimate is computed using following equation based on the nonlinear relationship

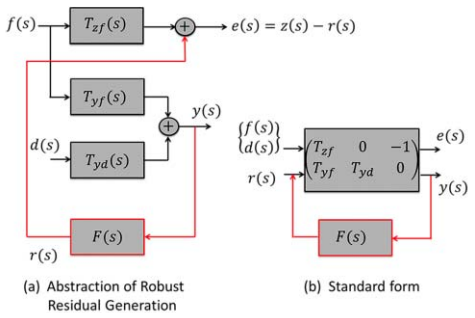

Fig. 17. Framework for robust residual generation.

between rotor speed and aerodynamic torque given in (1):

$$\hat{\tau}_{r,i} = F(\omega_{r,i} + \Delta\omega_{r,i}) \cong \tau_r + \chi\,\Delta\omega_{r,i} \tag{17}$$

where χ is the gradient function based on local linearization of the nonlinear map and $\Delta\omega_{r,i}$ is rotor speed sensor fault. After some manipulations, the rotor and generator speed sensor residuals can be written as

$$\begin{aligned} r_{\omega r1} &= (1 - T_{\omega_r\tau_r}(s)\chi)\Delta\omega_{r1} + \Delta T_{rg1}(s, \Delta\eta)\begin{bmatrix}\tau_r(s)\\ \tau_g(s)\end{bmatrix} \\ r_{\omega g1} &= -T_{\omega_g\tau_r}(s)\chi\,\Delta\omega_{r1} + \Delta\omega_{g1} \\ &\quad + \Delta T_{rg2}(s, \Delta\eta)\begin{bmatrix}\tau_r(s)\\ \tau_g(s)\end{bmatrix}. \end{aligned} \tag{18}$$

The isolation of the generator speed sensors can be done using the generator power sensor information. The following residuals are used for that purpose:

$$r_{\omega gPi} = \omega_{g,mi} - \frac{P_{g,m}}{\tau_{g,m}}, \quad i = 1, 2. \tag{19}$$

The residual for the actuator fault is given below

$$r_{\tau_g} = \tau_{g,m} - \frac{\alpha_{gc}}{s + \alpha_{gc}}\tau_{g,r}. \tag{20}$$

After generating the primary residuals, a secondary residual generation scheme is constructed by drawing on results from robust control theory [36]. The formulation of robust residual generation scheme is shown in Fig. 17.

Here, y is the primary residual vector, f is the fault vector, d is the disturbance vector, Z is the secondary residual vector which possesses desired characteristics of the residual, T_{zf} is the transfer matrix between the fault vector and secondary residual vector, T_{yf} is the transfer matrix between the fault vector and primary residual vector, and T_{yd} is the transfer matrix between the disturbance vector and primary residual vector. The objective here is to design the filter F, which takes the primary residual vector as input and outputs the secondary residual vector.

For the pair of rotor speed sensor 1 and generator speed sensor 1, the fault to primary residual transfer matrix is defined as

$$\begin{bmatrix} r_{\omega r1} \\ r_{\omega g1}\end{bmatrix} = \begin{bmatrix} (1 - T_{\omega_r\tau_r}(s)\chi) & 0 & T_{\omega_r\eta}(s) \\ -T_{\omega_g\tau_r}(s)\chi & 1 & T_{\omega_g\eta}(s)\end{bmatrix}\begin{bmatrix}\Delta\omega_{r1}\\ \Delta\omega_{g1}\\ \Delta\eta\end{bmatrix} \tag{21}$$

TABLE VIII
FAULT SIGNATURE TABLE FOR PARITY EQUATION/H_∞-BASED DIAGNOSIS SCHEME

Faults	Residuals						
	Secondary		Primary		From power /Torque Sensors		
	$r_{\omega r1f}$	$r_{\omega r2f}$	$r_{\omega g1}$	$r_{\omega g2}$	$r_{\omega gP1}$	$r_{\omega gP2}$	r_{τ_g}
$\omega_{r,m1}$ (stuck)	1	0	1	0	0	0	0
$\omega_{r,m2}$ (stuck)	0	1	0	1	0	0	0
$\omega_{r,m1}$ (gain)	1	0	0	0	0	0	0
$\omega_{r,m2}$ (gain)	0	1	0	0	0	0	0
$\omega_{g,m1}$ (stuck/gain)	0	0	0	0	1	0	0
$\omega_{g,m2}$ (stuck/gain)	0	0	0	0	0	1	0
$\tau_{g,m}$	0	0	0	0	0	0	1
η	0	0	1	1	0	0	0

where $T_{\omega_g\tau_r}(s)$ and $T_{\omega_r\tau_r}(s)$ are the nominal transfer functions. The transfer functions between the parametric (efficiency) fault to the residuals are computed by considering the perturbations of the nominal model with respect to the system efficiency given the nominal inputs. It can be shown that the resulting transfer functions take the form [37]

$$\begin{bmatrix} T_{\omega_r\eta}(s) \\ T_{\omega_g\eta}(s)\end{bmatrix} = C(sI - A)^{-1}\frac{\partial A}{\partial\eta}(sI - A)^{-1}B\begin{bmatrix}\bar{\tau}_r(s)\\ \bar{\tau}_g(s)\end{bmatrix}. \tag{22}$$

To accommodate the variation in the torque coefficient with different operating points of the wind turbine, a low-pass filter with a large break frequency λ and a real *uncertain* gain K is used in modeling χ

$$\chi(s) = \frac{K\lambda}{S + \lambda}, \quad K \in [-1.5, 7] \times 10^5.$$

As the generator speed sensor faults are determined using the generator torque and power measurements, the T_{yf} structure is used only to determine the rotor speed sensor faults and system efficiency fault. Finally, we define the specification of the transfer function from the fault to the secondary residual (incorporating desired decoupling behavior) as

$$T_{zf}(s) = \begin{bmatrix} \dfrac{\alpha_{\omega_r}^2}{(s + \alpha_{\omega_r})^2} & 0 & \dfrac{\alpha_{\omega_{r\eta}}}{s + \alpha_{\omega_{r\eta}}} \\ 0 & \dfrac{\alpha_{\omega_r}^2}{(s + \alpha_{\omega_r})^2} & \dfrac{\alpha_{\omega_{g\eta}}^2}{(s + \alpha_{\omega_{g\eta}})^2}\end{bmatrix}.$$

After setting up the standard from in Fig. 17(b), we can solve for the desired filter F using MATLAB's μ-*synthesis* toolbox. The fault signatures corresponding to the overall scheme are given in Table VIII. An example residual response

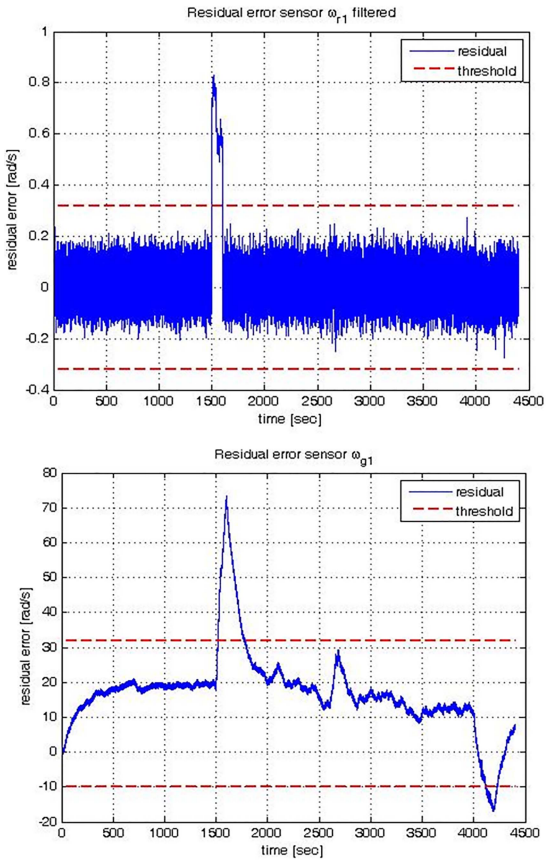

Fig. 18. Residual response (R_1) for rotor speed sensor 1 fault.

TABLE IX
SIMULATION RESULTS FOR DEDICATED OBSERVER-BASED DIAGNOSIS SCHEME

Fault Scenario	Detection/Isolation	Detection Time (s)
Simultaneous scaling error sensor faults of rotor speed sensor 2 and generator speed sensor 2	Detected, Isolated	0.11
Single sensor stuck fault of rotor speed sensor 1	Detected, Isolated	0.05 (D) /16.3 (I)
Bias fault in converter actuator	Detected, Isolated	0.01
Drivetrain efficiency change	Detected, Isolated	113.85

(corresponding to rotor speed sensor 1) is shown in Fig. 18. Results from applying this diagnosis scheme on the diagnostic problems described in Section III are listed in Table IX. Simulation sample time is 0.01 s.

V. ROBUSTNESS ANALYSIS AND COMPARISONS

A. Robustness Analysis

One important issue in the evaluation of diagnostic schemes is analysis of robustness. Here, we evaluate the three proposed schemes in three different ways: 1) we evaluate the schemes under parametric uncertainties by varying some important model parameters with respect to their nominal values; 2) we change the time occurrence of the faults and check the performance of the schemes under different operating conditions; and 3) the residual threshold values for the cascaded Kalman filter-based scheme are designed based on certain assumptions on noise and fault probability distributions. We analyze the effect of changes in fault sizes on the cascaded Kalman filter-based schemes.

First, we analyze the effect of parametric uncertainty on the schemes by conducting a Monte Carlo analysis with the following test cases.

Test Case 0: Nominal model parameters.
Test Case 1: Vary C_q 10%.
Test Case 2: Vary C_q 50%.
Test Case 3: Wind speed measurement bias 10%.
Test Case 4: Wind speed measurement bias 20%.
Test Case 5: B_r change 50%.
Test Case 6: B_g change 50%.
Test Case 7: B_{dt} change 50%.
Test Case 8: K_{dt} change 50%.

In the Monte Carlo analysis, we evaluate the following parameters as discussed in [8]: T_{dmax} is the maximum detection time in a test case, T_{dmin} is the minimum detection time in a test case, T_{davg} is the average detection time for a test case, FA_{max} is the maximum number of false alarms in a test case, FA_{min} is the minimum number of false alarms in a test case, FA_{avg} is the average number of false alarms in a test case, and M_D is the average percentage of missed detection in a test case. We refer to the fault scenarios given in Table I as fault 1, fault 2, fault 3, and fault 4 in that order. The result of the Monte Carlo analysis is given in Table X.

Some general observations can be summarized from the analysis. In general, the cascaded Kalman filter-based approach shows better performance under uncertainty than the other two approaches. As expected, the dedicated observer-based approach has very limited capability to handle uncertainties. Therefore, in most of the test cases, there was huge number of false alarms, which makes this approach ineffective under parametric uncertainty. The major uncertainties come from the uncertain torque coefficient and wind speed measurement. It is noted the Kalman filter-based approach is able to handle up to around 30% uncertainty in torque coefficient and 10% bias in wind speed measurement. The parity equation approach is able to handle around 15% uncertainty in torque coefficient and 10% bias in wind speed measurement. Above these limits, the schemes start producing a huge number of false alarms.

Next, we conducted the Monte Carlo analysis of the three schemes under different operating conditions. This is done using the following test cases.

Test Case 9: $+100$ s shift for all faults.
Test Case 10: -100 s shift for all faults.
Test Case 11: -200 s shift for all faults.
Test Case 12: -300 s shift for all faults.

The result of this analysis is shown in Table XI. In general, it is noticed that the performance of the schemes were satisfactory under these test cases. However, the detection time is affected in some of the test cases.

TABLE X
MONTE CARLO ANALYSIS FOR ROBUSTNESS EVALUATION
(IN CASE OF PARAMETRIC UNCERTAINTIES)

Fault	Cascaded Kalman Filter Scheme	Dedicated Observer Scheme	Parity Equation /H_∞ Scheme
1	Tdmax=0.1 s Tdmin=0.1 s Tdavg=0.1 s FAmax=45 FAmin=0 FAavg=13.5 MD=12.5%	Tdmax=80 s Tdmin=80 s Tdavg=80 s FAmax=176 FAmin=130 FAavg=156 MD=0%	Tdmax=0.13 s Tdmin=0.1 s Tdavg=0.11 s FAmax=21 FAmin=0 FAavg=5 MD=37.5%
2	Tdmax=0.1 s Tdmin=0.1 s Tdavg=0.1 s FAmax=8 FAmin=0 FAavg=3.75 MD=12.5%	Tdmax=7 s Tdmin=7 s Tdavg=7 s FAmax=233 FAmin=186 FAavg=205 MD=0%	Tdmax=0.01 s Tdmin=0.01 s Tdavg=0.01 s FAmax=60 FAmin=0 FAavg=23.6 MD=50%
3	Tdmax=0.1 s Tdmin=0.1 s Tdavg=0.1 s FAmax=0 FAmin=0 FAavg=0 MD=0%	Tdmax=0.01 s Tdmin=0.01 s Tdavg=0.01 s FAmax=0 FAmin=0 FAavg=0 MD=0%	Tdmax=0.01 s Tdmin=0.01 s Tdavg=0.01 s FAmax=0 FAmin=0 FAavg=0 MD=0%
4	Tdmax=80 s Tdmin=8.4 s Tdavg=27.8 s FAmax=50.75 FAmin=123 FAavg=0 MD=12.5%	Tdmax=22 s Tdmin=22 s Tdavg=22 s FAmax=245 FAmin=164 FAavg=210 MD=0%	Tdmax=116 s Tdmin=113 s Tdavg=115 s FAmax=155 FAmin=128 FAavg=139 MD=62%

TABLE XI
MONTE CARLO ANALYSIS FOR ROBUSTNESS EVALUATION
(IN CASE OF DIFFERENT OPERATING CONDITIONS)

Fault	Cascaded Kalman Filter Scheme	Dedicated Observer Scheme	Parity Equation /H_∞ Scheme
1	Tdmax=0.1 s Tdmin=0.1 s Tdavg=0.1 s FAmax=0 FAmin=0 FAavg=0 MD=0%	Tdmax=95 s Tdmin=76 s Tdavg=83 s FAmax=12 FAmin=0 FAavg=3.37 MD=0%	Tdmax=0.13 s Tdmin=0.08s Tdavg=0.1 s FAmax=0 FAmin=0 FAavg=0 MD=0%
2	Tdmax=0.1 s Tdmin=0.1 s Tdavg=0.1 s FAmax=0 FAmin=0 FAavg=0 MD=0%	Tdmax=10 s Tdmin=6 s Tdavg=8.2 s FAmax=0 FAmin=0 FAavg=0 MD=0%	Tdmax=0.04 s Tdmin=0.01 s Tdavg=0.03 s FAmax=60 FAmin=0 FAavg=0 MD=0%
3	Tdmax=0.1 s Tdmin=0.1 s Tdavg=0.1 s FAmax=0 FAmin=0 FAavg=0 MD=0%	Tdmax=0.01 s Tdmin=0.01 s Tdavg=0.01 s FAmax=0 FAmin=0 FAavg=0 MD=0%	Tdmax=0.01 s Tdmin=0.01 s Tdavg=0.01 s FAmax=0 FAmin=0 FAavg=0 MD=0%
4	Tdmax=11 s Tdmin=4 s Tdavg=7 s FAmax=0 FAmin=0 FAavg=0 MD=0%	Tdmax=32 s Tdmin=21 s Tdavg=25 s FAmax=0 FAmin=0 FAavg=0 MD=0%	Tdmax=160 s Tdmin=86 s Tdavg=116 s FAmax=0 FAmin=0 FAavg=0 MD=0%

In [24], five different schemes have been compared based on nominal test case and additional test cases with shifting time occurrence of the faults. We can compare the performance of our schemes with the ones given in [24] under time shifting of the fault occurrence (one may refer to the test cases 9–12 there). In terms of nominal detection time, for fault 1, cascaded Kalman filter approach and parity equation approach are comparable or faster than most of them, however, due to significant filtering, the dedicated observer-based approach is much slower than the rest. For fault 2, cascaded Kalman filter approach and parity equation approach are faster than most of them except for the estimation-based approach [18], and dedicated observer approach is slower due to previously mentioned filtering. For fault 3, detection times for most of the approaches are comparable with each other although cascaded Kalman filter approach is a little slower. In terms of false alarm and missed detections, all the three approaches perform satisfactorily proving their robustness with respect to the operating conditions.

Finally, we analyze the effectiveness of the cascaded Kalman filter-based approach by varying fault sizes. In this approach, the residual threshold values are selected based on some assumed probability distribution of the faulty and nonfaulty cases (Figs. 8–10). However, in reality the probability distribution for the faulty case may differ from the assumed one which in turn may lead to higher false alarms and missed detections. For illustration purposes, we choose the generator actuator fault. However, similar analysis can be extended to other faults too. In Fig. 19, the probability distributions for different fault sizes have been shown along with the nonfaulty case. Note that the residual threshold was selected as 50 N · m based on the faulty case of 100 N · m bias. Therefore, in cases of smaller fault sizes of 10 and 50 N · m, this threshold gives rise to very high missed detection

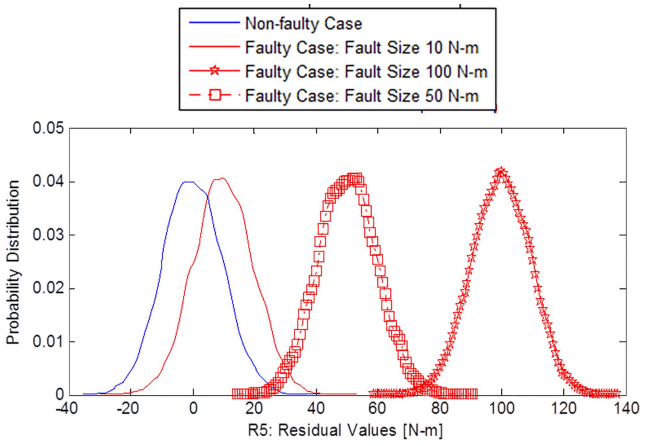

Fig. 19. Generator actuator fault residual probability distribution in faulty conditions with different fault sizes.

TABLE XII
COMPARISON OF DIAGNOSTIC SCHEMES

	Cascaded Kalman Filter Based Scheme	Dedicated Observer Based Scheme	Parity Equation/H_∞-Based Scheme
Detectability	Cannot detect faults with low fault-to-noise signal ratio	Can detect all kinds of faults considered in this paper. Additionally, can detect generator power sensor fault	Can detect all kinds of faults in this paper
Isolability	Can isolate all kinds of faults considered in this paper (except the faults with low fault-to-signal ratio)	Can isolate all kinds of faults considered in this paper	Can isolate all kinds of faults considered in this paper
Detection time	Fast	Much slower than the other two schemes.	Fast
Distinguishing fault type	Cannot distinguish	Cannot distinguish	Can distinguish gain-type or stuck-type fault
Tuning Effort	High	Low	High
Design Complexity	Moderate	Low	High
Computational Burden	Low	High	Low
Robustness to Parametric Uncertainties	Can handle parametric uncertainties to a certain extent (better than the other two schemes)	Performs degrades significantly under parametric uncertainties	Can handle parametric uncertainties to a certain extent (but less robust than cascaded Kalman filter approach)
Robustness to Operating Conditions	Robust to operating conditions	Robust to operating conditions	Robust to operating conditions

rates. One of the possible solutions for this issue could be choosing the residual threshold based on nonfaulty probability distribution (assuming the noise statistical properties are known) and the maximum allowable probability of false alarm rates. Note that in reality the faults will not be exactly the same as considered in the benchmark model. Therefore, it is important to have an estimate of the minimum detectable fault size. Using simulation studies, the approximate minimum detectable fault sizes are found for several faults: minimum detectable bias fault in generator actuator 25 $\mathrm{N}\cdot\mathrm{m}$, minimum detectable stuck fault in rotor speed sensor 1 rad/s, minimum detectable gain fault in rotor speed sensor 1.08, which is 8% deviation from the nominal gain. However, note that these values are only estimates and for more rigor, the minimum detectable fault sizes may be analyzed theoretically. An estimate of the minimum detectable fault size can be analyzed given an allowable probability of missed detections. Bias type of sensor fault changes the nonfaulty residual probability distribution by shifting its mean. Therefore, the faulty (p_f) and nonfaulty (p_0) probability distributions have same properties only shifted by mean. The probability of the missed detection can be calculated as: $P_{\mathrm{MD}} = \int_{-\infty}^{\mathrm{th}} p_f(x, f)dx$, where P_{MD} is the probability of missed detection, p_f is the faulty-probability distribution, f is the fault (which in this case is the mean of the p_f), and th is the threshold. Note that p_f is known from the nonfaulty probability distribution p_0 except for its mean which is the fault (for sensor bias fault, $p_f = p_0(x - f)$). If the allowable probability of missed detection is given (P_{MD_a}) and the threshold is selected ($\mathrm{th}_{\mathrm{sel}}$), then denoting $\int_{-\infty}^{\mathrm{th}} p_f(x, f)dx = F(\mathrm{th}, f)$, the minimum detectable fault can be calculated as: $f_{\min} = F^{-1}(\mathrm{th}_{\mathrm{sel}}, P_{\mathrm{MD}\_a})$. However, for nonlinear systems and other types of faults, this approach may not be valid. In some existing literature, such as [38] and [39], systematic approaches for analyzing minimum detectable fault have been given based on residual norm evaluation in the presence of modeling uncertainty and disturbances.

B. Comparative Discussions

A general comparison of the three proposed schemes is summarized in Table XII. The first scheme, which is based on cascaded Kalman filter, approach utilizes the difference between filter estimates and sensor measurements as residuals. The scheme seems to perform well in terms of detecting and isolating different faults, but the drawback is that the residuals directly depend on the sensor measurements. Therefore, in case of a sensor fault with very low fault-to-noise signal ratio, this scheme may fail to detect. It is evident from the simulation results that it could not detect the fault in rotor speed sensor 2 at 1000 s (Table IV). This scheme can be improved using a bank of Kalman filters each of which is tuned to be sensitive to a particular fault. In that case, the difference between different filter estimates can be used as residuals bypassing the dependence on the sensor information directly. However, this improvement will come at a cost of higher computational burden, as the number of filters increases and more rigorous tuning may be needed for each.

The second scheme, which is based on a bank of observers, utilizes the difference between different observer estimates as residuals. This scheme is able to detect even the faults with low fault-to-noise signal ratio. However, considerable amount of effort had to be spent in designing the second stage of filtering after the observer output to reduce the effects of noise

on the residuals. One of the advantages of this scheme is that it can also detect generator power sensor fault. The drawback of this scheme is that it is much slower than the other schemes due to low-pass filtering of the primary residuals. Due to this filtering in first stage of postprocessing, the residual settling time is long and creates an idle window after the fault is gone when the scheme is unable to detect any fault. The design challenge in this scheme lies in the tradeoff between the detectability of faults and speed of detection.

The third scheme is based on parity equation approach combined with robust filtering mechanism. This scheme performs fine in terms of detecting the faults and offers fast detection. This scheme is also better than the other two schemes in terms of distinguishing the fault type (gain type or stuck type). However, the design of the robust filtering scheme to accommodate the inherent nonlinearity, modeled here as an uncertainty and the subsequent selection of decoupling transfer matrices is a nontrivial task.

VI. Conclusion

A. Summary of Main Observations

In this paper, three different fault diagnosis schemes have been discussed to address the diagnostic problem for wind turbine drivetrain system. The first scheme utilizes a cascaded structure with two Kalman filters, the second scheme uses a set of dedicated Luenberger observers, and the third scheme uses a parity equation approach along with H_∞ filtering. All the three schemes have been tested via simulation studies. The cascaded Kalman filter-based approach and the parity equation approach are found to be faster in detecting the faults compared with the dedicated observer scheme. This is due to the significant filtering in the dedicated observer scheme. However, the Kalman filter-based approach is unable to detect faults with low fault-to-noise signal ratio. The robustness of the schemes is also analyzed in terms of parametric uncertainties and operating conditions. It is observed that the cascaded Kalman filter-based approach is more robust compared to the other two schemes under parametric uncertainties. Specifically, the dedicated observer-based scheme's performance degrades significantly under parametric uncertainties. However, all the three schemes are found to be robust in terms of change in operating conditions although the detection times are affected.

B. Discussions on Open Problems and Future Work

We conclude this discussion with some comments on the open problems of wind turbine diagnostics. One group of problems is the design and implementation of diagnostic scheme that will consider different combinations of simultaneous faults (actuator and sensor faults, actuator and system parametric faults, and different system parametric faults at the same time). In addition to that, system-level diagnostic problem can be extended considering faults in other sensors and actuators in wind turbine system (some examples are given in [9], such as blade root bending moment sensor, accelerometer, shaft position sensor, and yaw actuator fault). Robustness evaluation of the diagnosis schemes is important because unmodeled dynamics may significantly impact the performance of the schemes due to simplifications taken (such as the static aerodynamic model). Moreover, design of diagnostic scheme should be done considering more realistic wind scenario (an example of realistic wind scenario is given in enhanced benchmark model [9]). The next step following diagnostics is to design an active fault-tolerant control scheme for wind turbines, which is still an open research area [9]. Finally, experimental validation of these schemes on actual wind turbines is required to firmly establish their effectiveness.

References

[1] E. Hau, *Wind Turbines: Fundamentals, Technologies, Application and Economics*. 2nd ed. New York, NY, USA: Springer-Verlag, 2006.

[2] W. Yang, P. J. Tavner, and M. R. Wilkinson, "Condition monitoring and fault diagnosis of a wind turbine synchronous generator drive train," *IET Renew. Power Generat.*, vol. 3, no. 1, pp. 1–11, Mar. 2009.

[3] K. Rothenhagen and F. W. Fuchs, "Current sensor fault detection and reconfiguration for a doubly fed induction generator," in *Proc. IEEE Power Electron. Specialists Conf. (PESC)*, Jun. 2007, pp. 2732–2738.

[4] K. Rothenhagen, S. Thomsen, and F. W. Fuchs, "Voltage sensor fault detection and reconfiguration for a doubly fed induction generator," in *Proc. IEEE Int. Symp. Diagnostics Electr. Mach., Power Electron. Drives (SDEMPED)*, Sep. 2007, pp. 377–382.

[5] Q. Huang, D. Jiang, L. Hong, and Y. Ding, "Application of wavelet neural networks on vibration fault diagnosis for wind turbine gearbox," in *Advances in Neural Networks*. Berlin, Germany: Springer-Verlag, 2008, pp. 313–320.

[6] Z. Fucheng, "Fault diagnosis method of gear of wind turbine gearbox based on undecimated wavelet transformation," in *Proc. Int. Conf. Comput. Design Appl. (ICCDA)*, vol. 4. Jun. 2010, pp. V4-606–V4-609.

[7] P. F. Odgaard, J. Stoustrup, and M. Kinnaert, "Fault tolerant control of wind turbines a benchmark model," in *Proc. 7th IFAC Symp. Fault Detection, Supervision Safety Tech. Process.*, Barcelona, Spain, Jun./Jul. 2009, pp. 155–160.

[8] P. F. Odgaard, J. Stoustrup, and M. Kinnaert, "Fault-tolerant control of wind turbines: A benchmark model," *IEEE Trans. Control Syst. Technol.*, vol. 21, no. 4, pp. 1168–1182, Jul. 2013.

[9] P. F. Odgaard and K. E. Johnson, "Wind turbine fault detection and fault tolerant control—An enhanced benchmark challenge," in *Proc. Amer. Control Conf.*, Washington, DC, USA, Jun. 2013, pp. 4447–4452.

[10] T. Esbensen and C. Sloth, "Fault diagnosis and fault-tolerant control of wind turbines," M.S. thesis, Dept. Electron. Syst., Aalborg Univ., Aalborg, Denmark, Jun. 2009.

[11] S. Pourmohammad and A. Fekih, "Fault-tolerant control of wind turbine systems—A review," in *Proc. IEEE Green Technol. Conf. (IEEE-Green)*, Apr. 2011, pp. 1–6.

[12] S. Simani, P. Castaldi, and A. Tilli, "Data-driven approach for wind turbine actuator and sensor fault detection and isolation," in *Proc. IFAC World Congr.*, Milan, Italy, Aug./Sep. 2011, pp. 8301–8306.

[13] J. Dong and M. Verhaegen, "Data driven fault detection and isolation of a wind turbine benchmark," in *Proc. IFAC World Congr.*, Milan, Italy, Aug./Sep. 2011, pp. 7086–7091.

[14] N. Laouti, N. Sheibat-Othman, and S. Othman, "Support vector machines for fault detection in wind turbines," in *Proc. IFAC World Congr.*, Milan, Italy, Aug./Sep. 2011, pp. 7067–7072.

[15] F. Stoican, C. F. Raduinea, and S. Olaru, "Adaptation of set theoretic methods to the fault detection of wind turbine benchmark," in *Proc. IFAC World Congr.*, Milan, Italy, Aug./Sep. 2011, pp. 8322–8327.

[16] A. A. Ozdemir, P. Seiler, and G. J. Balas, "Wind turbine fault detection using counter-based residual thresholding," in *Proc. IFAC World Congr.*, Milan, Italy, Aug./Sep. 2011, pp. 8289–8294.

[17] W. Chen, S. X. Ding, A. Haghan, A. Naik, A. Q. Khan, and S. Yin, "Observer-based FDI schemes for wind turbine benchmark," in *Proc. IFAC World Congr.*, Milan, Italy, Aug./Sep. 2011, pp. 7073–7078.

[18] X. Zhang, Q. Zhang, S. Zhao, R. M. Ferrari, M. M. Polycarpou, and T. Parisini, "Fault detection and isolation of the wind turbine benchmark: An estimation-based approach," in *Proc. IFAC World Congr.*, Milan, Italy, Aug./Sep. 2011, pp. 8295–8300.

[19] F. Kiasi, J. Prakash, S. Shah, and J. Lee, "Fault detection and isolation of benchmark wind turbine using the likelihood ratio test," in *Proc. IFAC World Congr.*, Milan, Italy, Aug./Sep. 2011, pp. 7079–7085.

[20] P. F. Odgaard and J. Stoustrup, "Unknown input observer based detection of sensor faults in a wind turbine," in *Proc. IEEE Int. Conf. Control Appl.*, Yokohama, Japan, Sep. 2010, pp. 8–10.
[21] P. F. Odgaard and J. Stoustrup, "Fault tolerant control of wind turbines using unknown input observers," in *Proc. 8th IFAC Symp. Fault Detection, Supervision Safety Tech. Process. (SAFEPROCESS)*, vol. 8. Mexico City, Mexico, 2012, pp. 313–319.
[22] P. Pisu and B. Ayalew, "Robust fault diagnosis for a horizontal axis wind turbine," in *Proc. IFAC World Congr.*, Milan, Italy, Aug./Sep. 2011, pp. 7055–7060.
[23] D. Rotondo, F. Nejjari, V. Puig, and J. Blesa, "Fault tolerant control of the wind turbine benchmark using virtual sensors/actuators," in *Proc. 8th IFAC Symp. Fault Detection, Supervision Safety Tech. Process. (SAFEPROCESS)*, vol. 8. Mexico City, Mexico, 2012, pp. 114–119.
[24] P. F. Odgaard and J. Stoustrup, "Results of a wind turbine FDI competition," in *Proc. 8th IFAC Symp. Fault Detection, Supervision Safety Tech. Process. (SAFEPROCESS)*, vol. 8. Mexico City, Mexico, 2012, pp. 102–107.
[25] S. Donders, V. Verdult, and M. Verhaegen, "Fault detection and identification for wind turbine systems: A closed-loop analysis," M.S. thesis, Faculty Appl. Phys., Univ. Twente, Enschede, The Netherlands, Jun. 2002.
[26] X. Wei, M. Verhaegen, and T. van den Engelen, " Sensor fault diagnosis of wind turbines for fault tolerant," in *Proc. 17th IFAC World Congr.*, Seoul, Korea, Jul. 2008, pp. 3222–3227.
[27] X. Wei and M. Verhaegen, "Fault detection of large scale wind turbine systems: A mixed H_∞/H_- index observer approach," in *Proc. 16th Medit. Conf. Control Autom.*, 2008, pp. 1675–1680.
[28] M. Sami and R. J. Patton, "An FTC approach to wind turbine power maximisation via T-S fuzzy modelling and control," in *Proc. 8th IFAC Symp. Fault Detection, Supervision Safety Tech. Process. (SAFEPROCESS)*, vol. 8. Mexico City, Mexico, 2012, pp. 349–354.
[29] K. Z. Østergaard, P. Brath, and J. Stoustrup, "Estimation of effective wind speed," *J. Phys., Conf. Ser.*, vol. 75, no. 1, p. 012082, 2007.
[30] F. E. Thau, "Observing the state of non-linear dynamic systems," *Int. J. Control*, vol. 17, no. 3, pp. 471–479, 1973.
[31] K. E. Johnson, L. Y. Pao, M. J. Balas, and L. E. Fingersh, "Control of variable-speed wind turbines: Standard and adaptive techniques for maximizing energy capture," *IEEE Control Syst. Mag.*, vol. 26, no. 3, pp. 70–81, Jun. 2006.
[32] H. Chingiz and F. Caliskan, *Fault Diagnosis and Reconfiguration in Flight Control Systems*, vol. 2. New York, NY, USA: Springer-Verlag, 2003.
[33] A. J. Krener, "The convergence of the extended Kalman filter," in *Directions in Mathematical Systems Theory and Optimization*. Berlin, Germany: Springer-Verlag, 2003, pp. 173–182.
[34] K. Reif, S. Gunther, E. Yaz, and R. Unbehauen, "Stochastic stability of the discrete-time extended Kalman filter," *IEEE Trans. Autom. Control*, vol. 44, no. 4, pp. 714–728, Apr. 1999.
[35] R. N. Claek, "Instrument fault detection," *IEEE Trans. Aerosp. Electron. Syst.*, vol. AES-14, no. 3, pp. 456–465, May 1978
[36] M. Blanke, M. Kinnart, J. Lunze, M. Staroswiecki, and J. Shroder, *Diagnosis and Fault-Tolerant Control*. New York, NY, USA: Springer-Verlag, 2003.
[37] D. S. Bernstein, *Matrix Mathematics: Theory, Facts, and Formulas With Application to Linear Systems Theory*, 1st ed. Princeton, NJ, USA: Princeton Univ. Press, 2005.
[38] A. Emami-Naeini, M. M. Akhter, and S. M. Rock, "Effect of model uncertainty on failure detection: The threshold selector," *IEEE Trans. Autom. Control*, vol. 33, no. 12, pp. 1106–1115, Dec. 1988.
[39] X. Ding, L. Guo, and P. M. Frank, "A frequency domain approach to fault detection of uncertain dynamic systems," in *Proc. 32nd IEEE Conf. Decision Control*, Dec. 1993, pp. 1722–1727.

Satadru Dey (S'14) received the B.Tech. degree in electronics and instrumentation engineering from the University of Kalyani, Kalyani, India, in 2008, and the M.Tech. degree in control systems from IIT Kharagpur, Kharagpur, India, in 2010. He is currently pursuing the Ph.D. degree with the Department of Automotive Engineering, Clemson University, Clemson, SC, USA.

His current research interests include control, estimation, and diagnostics of energy and transportation systems.

Mr. Dey is a Student Member of the American Society of Mechanical Engineers and the IEEE Control System Society. He was a recipient of the U.S. Department of Energy Graduate Automotive Technology Education Fellowship Award.

Pierluigi Pisu (M'07) was born in Genoa, Italy, in 1971. He received the Ph.D. degree in electrical engineering from Ohio State University, Columbus, OH, USA, in 2002.

He is currently an Associate Professor with the Department of Automotive Engineering, Clemson University, Clemson, SC, USA, where he holds a joint appointment with the Department of Electrical and Computer Engineering. He was involved in the area of sliding mode control and robust control. He was granted three U.S. patents in the area of model-based fault diagnosis in 2004. His current research interests include fault diagnosis with application to vehicle systems, and energy management control of hybrid electric vehicles.

Prof. Pisu is a member of the American Society of Mechanical Engineers and the Society of Automotive Engineers. He was a recipient of the 2000 Outstanding Ph.D. Student Award from the Ohio State University Chapter of the Honor Society of Phi Kappa Phi.

Beshah Ayalew received the M.S. and Ph.D. degrees in mechanical engineering from Penn State University, State College, PA, USA, in 2000 and 2005, respectively.

He is currently an Associate Professor of Automotive Engineering and the Co-Director of the DOE GATE Center of Excellence in Sustainable Vehicle Systems with the Clemson University-International Center for Automotive Research, Greenville, SC, USA. His current research interests include control systems and dynamics with applications in vehicle dynamics, manufacturing processes, and energy systems.

Dr. Ayalew was a recipient of the SAEs Ralph R. Teetor Educational Award in 2014, the Clemson University Board of Trustees Award for Faculty Excellence in 2012, and the National Science Foundation CAREER Award for his work in mobile control of distributed parameter systems in 2011. He was also a recipient of the Penn State Alumni Association Dissertation Award in 2005. He is an active member of the ASME Vehicle Design Committee, the IEEE Control Systems Society, and the Society of Automotive Engineers.